PALEOCEANOGRAPHY, VOL. 19, PA4006, doi:10.1029/2003PA000964, 2004

Oceanic forcing of interannual and multidecadal climate variability in the southwestern Indian Ocean: Evidence from a 160 year coral isotopic record (La Réunion, 55°E, 21°S)

Miriam Pfeiffer, Oliver Timm, and Wolf-Christian Dullo
Leibniz Institut für Meereswissenschaften, IFM-GEOMAR, Kiel, Germany

Steffen Podlech
Geological Survey of Denmark and Greenland, Copenhagen, Denmark

Received 10 September 2003; revised 3 June 2004; accepted 6 August 2004; published 13 October 2004.

[1] We have developed a new 163-year bimonthly coral $\delta^{18}O$ record from La Réunion (55°E, 21°S). Interannual variations in coral $\delta^{18}O$ are coherent with the Southern Oscillation Index but not with regional sea surface temperature (SST). Correlations with the global SST field suggest more negative seawater $\delta^{18}O$ ($\delta^{18}O_{sw}$) during La Niña years. We propose that the signal results from changes in the strength of the South Equatorial Current and the Indonesian throughflow, which carry low salinity water. Multidecadal variations in coral $\delta^{18}O$ are coherent with regional SST, but the sign is of opposite sense as expected from the coral $\delta^{18}O$-temperature relationship. This requires multidecadal changes in salinity large enough to overprint the SST contribution in the coral $\delta^{18}O$ record. Our results suggest that multidecadal salinity variations result from modulations in the transport of the South Equatorial Current, which varies in response to the surface wind field and/or the Indonesian throughflow. *INDEX TERMS:* 1040 Geochemistry: Isotopic composition/chemistry; 3344 Meteorology and Atmospheric Dynamics: Paleoclimatology; 4215 Oceanography: General: Climate and interannual variability (3309); 4267 Oceanography: General: Paleoceanography; 4522 Oceanography: Physical: El Nino; *KEYWORDS:* corals, oxygen isotopes, Indian Ocean

Citation: Pfeiffer, M., O. Timm, W.-C. Dullo, and S. Podlech (2004), Oceanic forcing of interannual and multidecadal climate variability in the southwestern Indian Ocean: Evidence from a 160 year coral isotopic record (La Réunion, 55°E, 21°S), *Paleoceanography*, *19*, PA4006, doi:10.1029/2003PA000964.

1. Introduction

[2] In the past decades there has been great interest in the use of geochemical parameters measured in corals as paleoclimatological indicators. Corals have proven to be particularly useful for examining past climatic variability in the tropical oceans on interannual to centennial timescales [e.g., *Cole et al.*, 1993; *Charles et al.*, 1997; *Ren et al.*, 2002; *Charles et al.*, 2003]. The stable oxygen isotopic composition of coral skeletons records both variations in sea surface temperature (SST) [e.g., *Charles et al.*, 1997] and the isotopic composition of seawater ($\delta^{18}O_{sw}$) [e.g., *Cole et al.*, 1993; *Ren et al.*, 2002]. Both SST and $\delta^{18}O_{sw}$ are important climatic parameters. $\delta^{18}O_{sw}$ is related to the hydrological balance and oceanographic circulation and covaries with sea surface salinity (SSS) [*Craig and Gordon*, 1965]. High-resolution proxy data from corals can be used to extend short instrumental records of SST or SSS to several centuries, and may also provide a database for the reconstruction of climate fields in the preinstrumental period [*Evans et al.*, 2000, 2002].

[3] In the southern subtropical Indian Ocean, where rainfall is weak, evaporation exceeds precipitation in the annual mean [*Han and McCreary*, 2001]. Evaporation from the ocean surface maintains abundant water vapor in the atmospheric column [*Hastenrath and Greishar*, 1993]. A large proportion of the moisture evaporated during the boreal summer is carried northward across the equator in the lower-layer monsoon flow. The southern tropical Indian Ocean (10°–30°S) appears to provide the major moisture supply for the release of precipitation over Southern Asia during the Southwest Monsoon [*Hastenrath and Greischar*, 1993; *Wajsowicz and Schopf*, 2001]. *Wajsowicz and Schopf* [2001] suggest that the amount of evaporation over the southern Indian Ocean is influenced by the Indonesian throughflow. The throughflow water enters the eastern Indian Ocean between 9° and 12°S, and is advected toward Africa within the South Equatorial Current (SEC). Eventually, the throughflow water exits the western Indian Ocean within the Agulhas Current. The Indonesian throughflow-SEC Agulhas current system is a major component in global climate, transporting heat and freshwater from the equatorial Pacific to the southwestern Indian Ocean and, eventually, into the Atlantic [*Godfrey*, 1996; *DiMarco et al.*, 2002].

[4] Observational and model studies suggest that the transport of the Indonesian throughflow varies significantly with the phase of the El Niño–Southern Oscillation (ENSO), with larger transport during La Niña, and reduced transport during El Niño events [e.g., *Meyers*, 1996; *Godfrey*, 1996; *Gordon and McClean*, 1999]. Historical salinity data from the western Indian Ocean show ENSO-

0883-8305/04/2003PA000964$12.00

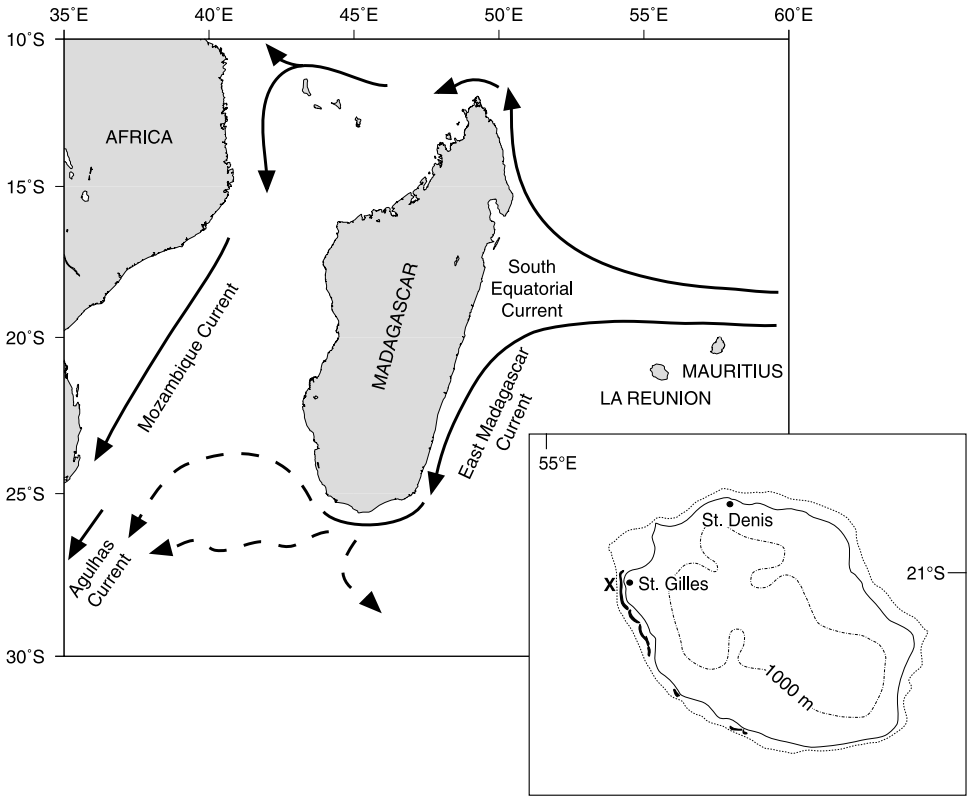

Figure 1. Map of the southwestern Indian Ocean with major oceanic surface currents (redrawn from *DiMarco et al.* [2002]). Inset: map of La Réunion. Location of coral core is marked with an "x." Coral reefs (black) and approximate 100 m isobath (dashed line) are indicated.

related variations in SSS [*Rao and Sivakumar*, 2003]. Previous studies based on instrumental data have also identified significant multidecadal variability in the southern Indian Ocean [e.g., *Allan and Haylock*, 1993; *Allan et al.*, 1995; *Reason et al.*, 1996; *Reason*, 2000], which may have arisen through a combination of: (1) basin-scale atmosphere-ocean interactions modulating the strength of the south Indian ocean gyre [*Reason et al.*, 1996, 1998], (2) remote forcing via variations in the Indonesian throughflow [*Reason et al.*, 1996], (3) variations in the surface heat fluxes in response to the local wind forcing [*Reason*, 2000].

[5] In this paper we present a new subseasonal coral $\delta^{18}O$ record (1832–1995 A. D.) developed from a *Porites* coral drilled off the west coast of La Réunion. Réunion is situated in the southwestern, subtropical Indian Ocean and lies within the path of the SEC, which carries the bulk of the water form the Indonesian throughflow. Through comparison with instrumental climate data, we will (1) evaluate the relative contribution of SST and $\delta^{18}O_{sw}$ to the coral isotopic signal (2) discuss the impact of local, regional and large-scale climate fluctuations on coral $\delta^{18}O$, and (3) propose possible forcing mechanisms.

2. Regional Setting

[6] Réunion is the most southwesterly of the Mascarene Islands and is situated about 800 km east of Madagascar. It is the youngest island of the Mascarene group, and has its highest peak with 3069 m. Compared to the other Mascarene islands, reef development is poor. Only 10–12 km of fringing reef are found on the southwest coast (Figure 1).

[7] Réunion lies within the path of the SEC, flowing westward between about 10°S and 20°S (Figure 1). The current appears to be unaffected by the presence of Réunion island [*Leroy and Barbaroux*, 1980]. The SEC forms the northern limb of the subtropical Indian Ocean gyre, and is the most powerful and persistent current in the Indian Ocean, being joined and strengthened by the Indonesian throughflow [*Wajsowicz*, 2002]. The SEC bifurcates near the midpoint of the east Madagascan coast, and the southward flowing branch, known as the East Madagascar current, feeds the Agulhas current (Figure 1). The northern limb of the SEC rounds the northern tip of Madagascar, and turns southward to become the Mozambique current, although part of it continues north [*DiMarco et al.*, 2002].

[8] The climate of Réunion is dominated by the southeasterly trade winds, which are blowing year-round from a generally east-southeastern direction (Figure 2a). The SE trade winds are strongest in austral winter, lasting from May to October. During this time of the year, the Intertropical Convergence Zone (ITCZ) is situated over the Indian subcontinent. In austral summer, the SE trades are weaker. The ITCZ forms south of the equator, occasionally influ-

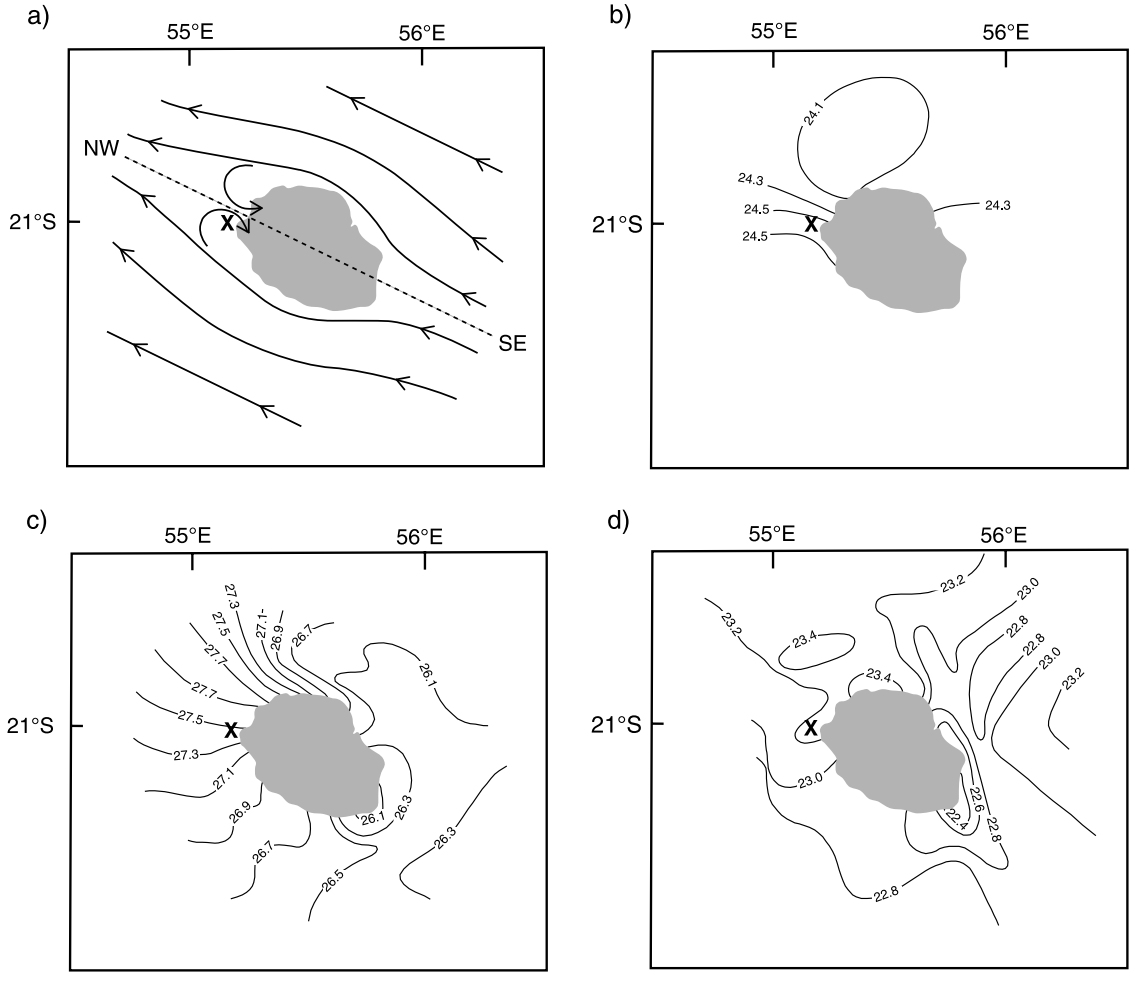

Figure 2. (a) Surface wind field in the vicinity of La Réunion; (b) surface isotherms (°C) in August 1977 [after *Leroy and Barbaroux*, 1980]; (c) surface isotherms (°C) in April 1979 [after *Leroy and Barbaroux*, 1980]; (d) surface isotherms (°C) in August 1982 [after *Gamberoni et al.*, 1984].

encing Réunion, causing periods of intense precipitation [*Soler*, 1997].

[9] SST has an average annual variation of 4.3°C, with minima of 23.5°C in August/September, and maxima of 27.8°C in February [*Conkright et al.*, 2002]. Average SSS varies by <0.3 psu annually, ranging from 34.9 psu in April to 35.2 psu in November [*Conkright et al.*, 2002]. The seasonal precipitation-evaporation balance (P-E) varies from −50 to −100 mm/month in June–October to +100 mm/month in January–March [*Oberhuber*, 1988].

[10] Réunion lies at a major shipping route and has excellent instrumental climate data (Figure 3). A local air temperature record from the capital St. Denis extends to 1951 (available through http://ingrid.ldgo.columbia.edu/), and rainfall records extend until 1911 [*Hulme*, 1992].

[11] The high relief of Réunion causes pronounced windward/leeward effects (Figure 2). Rainfall is extremely high, but the magnitude is unrepresentative of the surrounding ocean area [*Stoddart*, 1971]. Abundant precipitation (4–10 m/year) occurs on the windward side (southeast coast), whereas the leeward side of the island is much drier (1–2 m/year) [*Soler*, 1997]. XBT data around Réunion were collected at less than 35 miles from the coast during three cruises [*Leroy and Barbaroux*, 1980; *Gamberoni et al.*, 1984]. The XBT data show much higher SSTs on the leeward side of the island, where the coral reefs have developed, and colder SSTs on the windward side (Figures 2c and 2d). In August 1977, the SST gradients expected from local wind forcing were reversed (Figure 2b). Temperature/salinity relationships showed two distinct water masses separated by a density gradient [*Leroy and Barbaroux*, 1980]. These small-scale SST patterns are not resolved in gridded SST data.

[12] To assess the importance of windward-leeward effects, we compared the St. Denis air temperature and precipitation records with the relevant optimal smoothed (OS) SST from the *Kaplan et al.* [1998] data set. The OS SST has a spatial resolution of 5° × 5° degrees. The correlation between local air temperature and regional SST is high ($r = 0.64$, $p < 0.001$). Deviations due to windward/leeward effects appear to be limited to seasonal timescales. Similar results (not shown) were obtained when

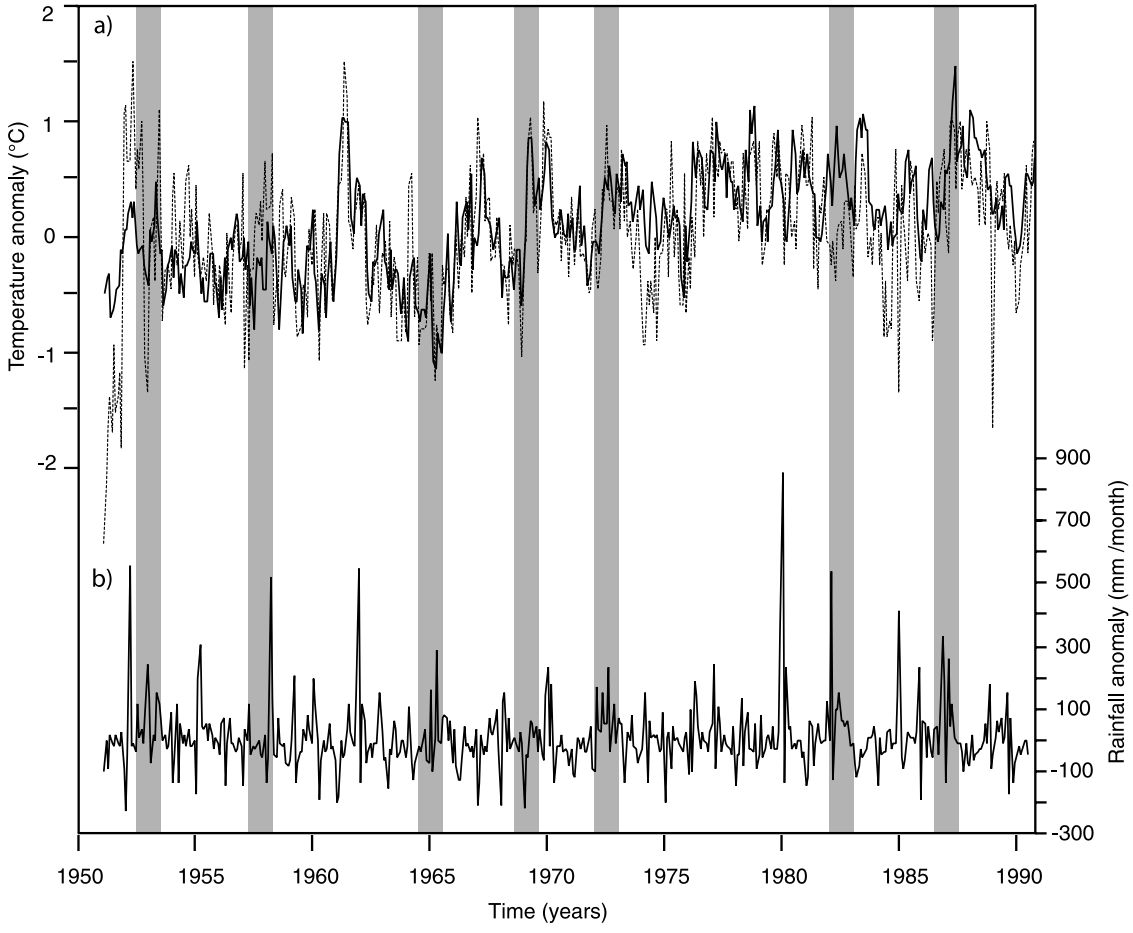

Figure 3. (a) Monthly sea surface temperature anomalies from the *Kaplan et al.* [1998] data set (solid line) compared with local air temperature anomalies from St. Denis weather station (dashed line; data available at http://ingrid.ldgo.columbia.edu). (b) Monthly rainfall anomalies [*Hulme*, 1992]. Shaded areas: El Niño years [after *Quinn and Neal*, 1992].

using the SST from the GISST 2.3 data set [*Parker et al.*, 1995].

3. Material and Methods

3.1. Coral Sampling

[13] In October 1995, a 1.95 m core was retrieved from a *Porites sp.* colony living at the outer reef slope in a water depth of 12.3 m. The site is located approximately 1 km offshore of St. Gilles (Figure 1). The core was drilled parallel to the dominant axis of growth using a pneumatique drill with a 3.6 cm inner diameter core barrel. The coral core was rinsed in freshwater, air dried and cut into 5 mm thick slabs. The slabs were cleaned in an ultrasonic bath with deionized water to remove saw cuttings and were then oven dried at 40°C. The slabs were X-rayed to reveal annual density bands (Figure 4).

[14] Samples for stable isotope analysis were collected along the maximum axis of growth using a 0.6 diameter diamond drill connected to a computer-aided drilling device (Figure 4). The top of the coral (1995–1976) was sampled at 1 mm increments, which yielded on average 11–12 samples per year, to facilitate calibration with monthly resolved SST data. The remaining part of the coral core was sampled at 5–7 samples per year. As the density bands revealed a decrease in coral growth rates from ~11 mm between 1996 and 1900 to 5–8 mm prior to 1900, samples were taken at 2 mm increments in the upper, and 1 mm increments in the lower part of the coral.

[15] The powdered samples were reacted with 100% H_3PO_4 at 68°C in an online, automated carbonate preparation device (Kiel device). The resulting CO_2 gas was analyzed using a Finnigan Mat 252 mass spectrometer at the Geology Department of the University of Erlangen. The standard deviation of multiple samples (N = 267) of the international reference NBS-19 was ±0.06‰ for $\delta^{18}O$. All data are reported relative to Vienna Peedee belemnite (VPDB).

[16] The analytical error of the isotopic determination applies to single measurements. The measurement errors of any two isotopic determinations are independent, and the mean error reduces according to the formula:

$$\sigma_{\text{Total}}\left(\sigma^2/\text{N}\right)^{1/2},$$

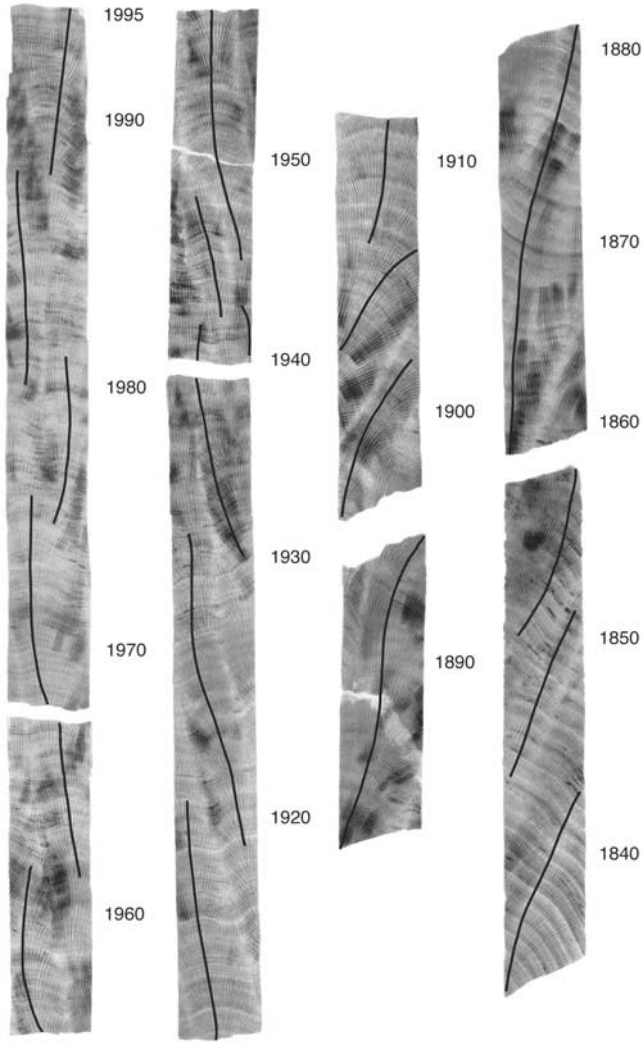

Figure 4. Xray of the coral core. Sampling paths for stable isotope analysis are indicated by the thick black line. Note the overall goodness of fit between individual slabs.

where N is the number of independent measurements and σ the analytical error. For annual mean $\delta^{18}O$ values calculated from six bimonthly values, the total analytical uncertainty reduces to ±0.024‰. For 11-year averages the uncertainty reduces to ±0.007‰.

3.2. Coral Chronology

[17] A first chronology was developed based on the density bands evident in the X-rays, which are presumed to represent one year of growth (Figure 4). The age model was then refined using the strong annual cycle in coral $\delta^{18}O$ (Figures 5 and 6). The heaviest isotopic value in any given year was assigned to 1 September, which is, on average, the coldest month. We then interpolated linearly between these anchor points into 12 equidistant points per year for the monthly, and 6 points per year for the bimonthly resolved series (Figure 5). This potentially creates a noncumulative error of ±1 month (monthly resolution) or ±2 month (bimonthly resolution) in any given year. In skeletal portions with unclear density banding (1900–1880), the age model is based solely on the strong annual cycle in coral $\delta^{18}O$. The overall goodness of fit between individual coral slabs suggests that the chronology is correct within ±1 years (Figure 4).

[18] Annual means were computed by averaging 6 bimonthly values (March/April to January/February). This is more appropriate than January to December in the tropics [*Ropelewski and Halpert*, 1987].

3.3. Time Series Analysis

[19] To ensure the stability of the spectral features observed in the coral record, we used three independent techniques of spectral analysis: the multitaper method (MTM) [*Thomson*, 1982], Wavelet analysis [*Torrence and Compo*, 1998], and Singular spectrum analysis (SSA) [*Vautard and Ghil*, 1989]. Cross-spectral analysis was performed via the Blackman-Tuckey method using the Analyseries software package [*Paillard et al.*, 1996].

[20] MTM and SSA were computed with the SSA-MTM Toolkit written by *Dettinger et al.* [1995]. MTM is a refinement of classical Fourier analysis, with optimal properties with respect to resolution and spectral leakage. *Mann and Lees* [1996] developed techniques that allow a robust signal detection against a red noise background. SSA allows the decomposition a time series into trend, oscillating and noise components by analyzing its covariance matrix [*Vautard and Ghil*, 1989]. *Allan and Smith* [1996] developed a method for calculating significance tests against a red noise background (Monte Carlo SSA).

[21] Wavelet power spectra were computed using the software of *Torrence and Compo* [1998]. This software provides a method of calculating significance levels of the wavelet moduli. Wavelet analysis was performed using the Morlet Wavelet. Significance levels were calculated against a red noise spectrum.

4. Results

[22] Measured $\delta^{18}O$ values ranged from −5.15 to −3.18‰ and show strong seasonal variations. Figure 5 compares monthly and bimonthly resolved coral $\delta^{18}O$ time series for the period 1973 to 1995, the latter computed by discarding every second value from the raw data to obtain a physical sample spacing of 2 mm, and then interpolating the series into 6 equidistant points per year. The mean amplitude of the annual cycle is 0.81‰ for the monthly resolved time series (Figure 5). The mean amplitude of the bimonthly resolved $\delta^{18}O$ series is 0.66‰, which equals 81% of the monthly series. Annual mean coral $\delta^{18}O$ values computed from the monthly and bimonthly data sets are nearly identical (Figure 5). The complete, bimonthly resolved record extends from 1995 to 1832 (Figure 6). The largest negative $\delta^{18}O$ anomalies occurred in 1940–1941. The long-term trend in coral $\delta^{18}O$ shows an almost linear decrease of 0.7‰ since 1830. Mean coral growth increased from 5–8 mm/year prior to 1900 to 9–12 mm/year from 1900–1995. Over the full record, the correlation between annual mean coral $\delta^{18}O$ and coral growth rates is $r = 0.65$ ($p < 0.001$). There is no significant

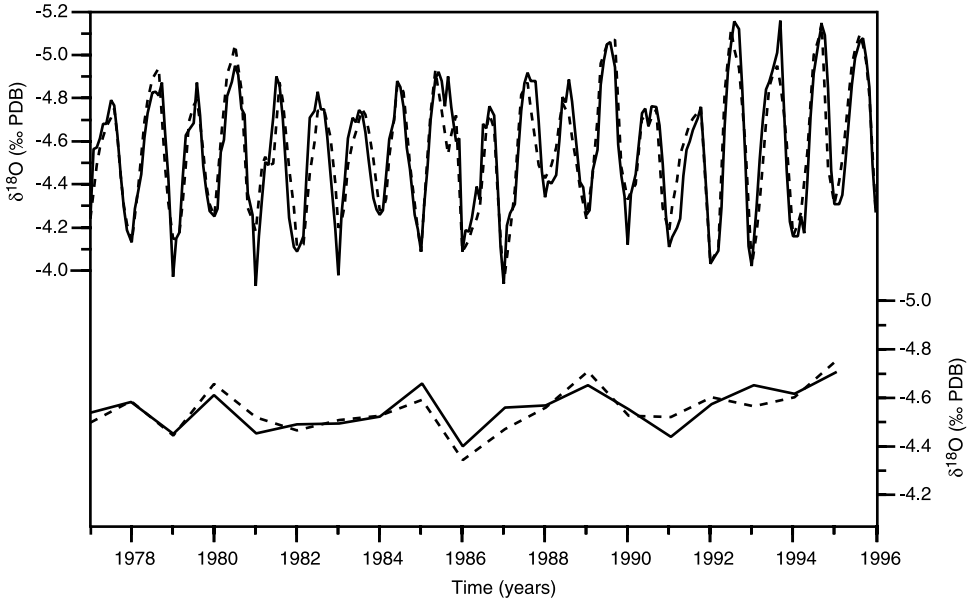

Figure 5. The upper curve shows the comparison of monthly and bimonthly resolved coral $\delta^{18}O$ time series for the period 1977–1995. The lower curve shows the annual means computed from the monthly and bimonthly $\delta^{18}O$ time series.

correlation between the detrended records of $\delta^{18}O$ and skeleton extension rate.

[23] To characterize our results in the frequency domain, we applied several independent methods of spectral analysis to the detrended, annual mean coral $\delta^{18}O$ time series (Figure 7). Multitaper spectral analysis shows significant (95%) spectral peaks centered at periods 35, 6.3–7.2 and 3.7 years (Figure 7a). Wavelet analysis reveals a highly variable spectrum with strongest variability in the pre-1920 period. Significant variability (at the 95% confidence level) is centered approximately at periods 30–34 and 6–8 years (Figure 7b). Variability in the 3–4 year periodicity band is only locally significant. Monte Carlo SSA (Figure 7c) indicates that the 6–7 year oscillation is the most robust

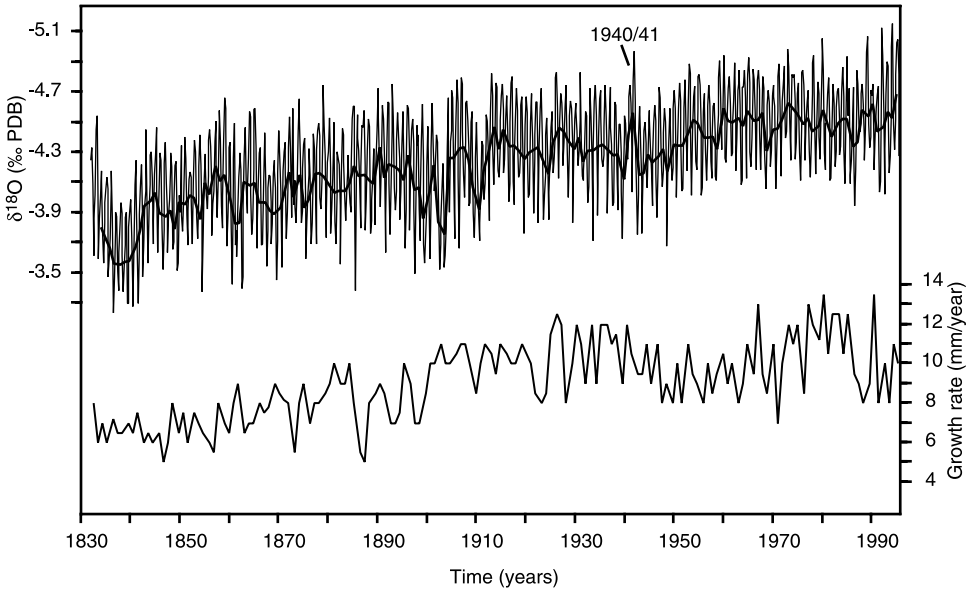

Figure 6. The upper curve shows the bimonthly $\delta^{18}O$ series (thin line) for the period 1832–1995 and annually averaged $\delta^{18}O$ series (thick line) calculated from the bimonthly series. Note large negative $\delta^{18}O$ anomaly in 1940/1941. The lower curve shows the mean annual coral growth rates.

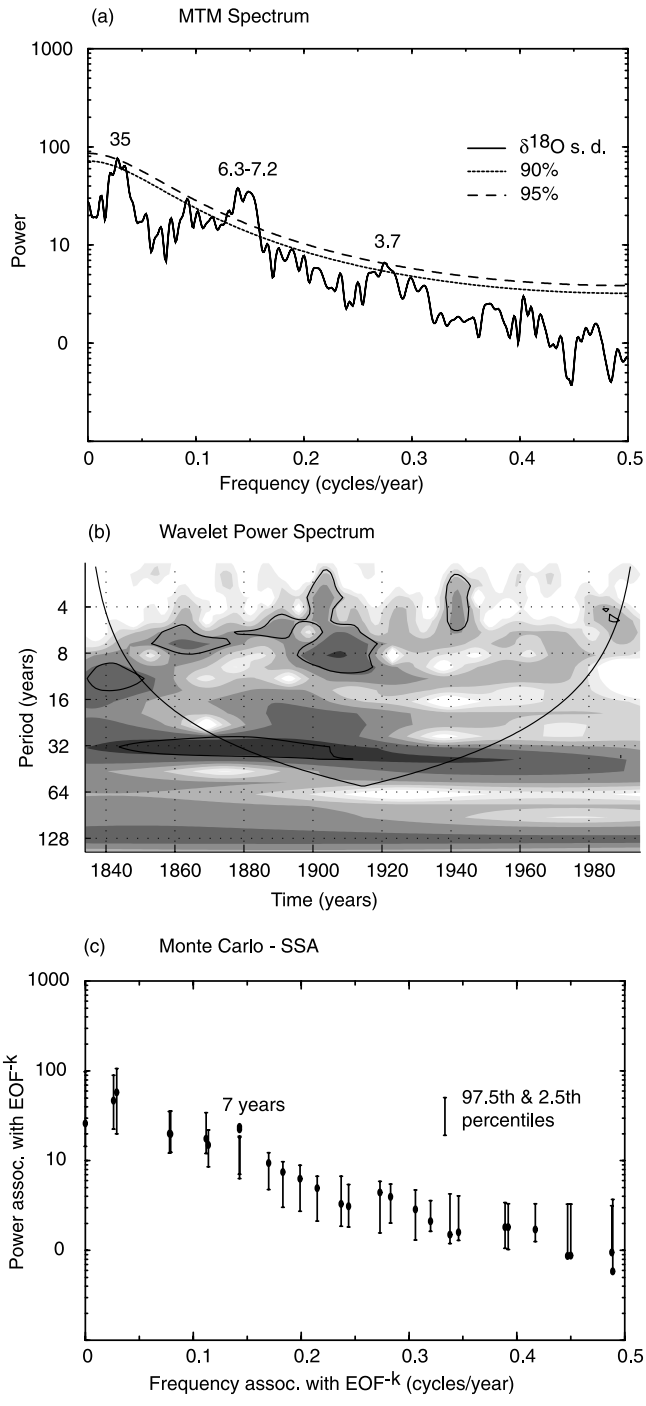

Figure 7. Time series analysis of the annual mean coral $\delta^{18}O$ series (detrended, normalized). (a) MTM spectrum with 90% and 95% confidence levels indicated. Periods (years) of significant spectral peaks are shown. (b) Morlet wavelet power spectrum. Solid line indicates 95% confidence level. Stippled line delineates cone of influence, where edge effects reduce the variance. (c) Monte Carlo SSA. Only the 6–7 year oscillation lies above the 97.5th percentile. See text for discussion.

feature of the coral record (significant above the 97.5th percentile).

5. Discussion

5.1. Calibration With the SST Record

[24] There is no local SST record, which comes directly from our coral site. Hence a calibration of our coral record must rely on the relevant grid box of global SST data sets. To assess the importance of local windward/leeward effects (Figure 2), we computed the correlation between monthly air temperature anomalies (mean seasonal cycle removed) from St. Denis weather station and gridded SST anomalies from the Kaplan data set (Figure 3). The correlation is high ($r = 0.64$, $p < 0.001$). For annual means, the correlation improves to $r = 0.75$ ($p < 0.001$) (not shown). We would expect to find the same correlation between annual mean coral $\delta^{18}O$ and gridded SST, provided that the coral record shows temperature (St. Denis is also located on the leeward side of Réunion island).

[25] Correlations between the instrumental temperature records and our proxy series were evaluated using standard ordinary least squares regression (OLS). We used NCEP [*Reynolds and Smith*, 1994], COADS [*Woodruff et al.*, 1987] and GISST 2.3 [*Parker et al.*, 1995] SST data sets, all having various spatial resolutions and spanning different time intervals (Table 1). In a first step, we calibrated the coral $\delta^{18}O$ time series with SST with the seasonal cycle included. For comparison with the bimonthly resolved coral $\delta^{18}O$ time series, the SST data were translated to bimonthly resolution by averaging two sequential monthly values. The correlation between monthly and bimonthly coral $\delta^{18}O$ and SST is high because of the pronounced seasonal cycle in both the instrumental and proxy data (Table 1). The slopes of the $\delta^{18}O$/temperature calibrations depend on the data sets used, but range between 0.18 and 0.21‰/°C. They fall well within the range of published coral $\delta^{18}O$/temperature relationships for *Porites* corals, ranging from 0.18 to 0.22‰/°C [*Gagan et al.*, 1994; *Wellington et al.*, 1996; *Juillet-Leclerc and Schmidt*, 2001]. The slope values suggest that on a seasonal scale, coral $\delta^{18}O$ is primarily a function of SST. (The effects of the seasonal SST and P-E balance on coral $\delta^{18}O$ should be additive. If the freshwater flux would measurably influence coral $\delta^{18}O$, we would expect an amplification of the $\delta^{18}O$ signal with respect to temperature.)

[26] In a second step, we compared the annual mean coral $\delta^{18}O$ computed from the monthly and bimonthly time series with annual mean SST. There is no statistically significant correlation between annual mean coral $\delta^{18}O$ and regional SST, regardless of the data sets used (Table 1). The correlation coefficient of the mean annual $\delta^{18}O$/SST calibration varies from positive to negative (Table 1), depending on the SST data set. There is also no significant correlation between annual mean coral $\delta^{18}O$ and local air temperature from the St. Denis weather station ($r = -0.2$, not significant). Therefore this misfit can not be explained with local, site-specific temperature variations.

[27] We conclude that the influence of SST on coral $\delta^{18}O$ is more or less negligible on timescales longer than the seasonal cycle. This requires changes in $\delta^{18}O_{sw}$ and SSS,

Table 1. Linear, Zero Lag, OLS Regression Equations Between Coral $\delta^{18}O$ and Sea Surface Temperature (SST)

Data Set	Resolution	SST Regression Equation	r (r^2)	Mean Annual r
		NCEP		
1995–1982	monthly	$-4.76(\delta^{18}O) + 3.78$	−0.81(0.66)	−0.11
1995–1982	bimonthly	$-5.22(\delta^{18}O) + 1.83$	−0.80(0.64)	−0.17
		COADS		
1992–1976	monthly	$-5.07(\delta^{18}O) + 2.66$	−0.82(0.67	0.08
1992–1963	bimonthly	$-5.42(\delta^{18}O) + 1.01$	−0.81(0.66)	−0.14
		GISST 2.3		
1995–1976	monthly	$-4.76(\delta^{18}O) + 4.36$	−0.83(0.69)	0.13
1995–1963	bimonthly	$-5.19(\delta^{18}O) + 2.42$	−0.82(0.68)	−0.02
1995–1871	bimonthly	$-3.88(\delta^{18}O) + 8.74$	−0.68(0.47)	−0.20

that are proportionally larger with respect to temperature at interannual and longer timescales, and dominate the annual mean coral record. This has also been found at other sites [*LeBec et al.*, 2000; *Lough*, 2004]. Variations in $\delta^{18}O_{sw}$ and SSS are not necessarily covariant with local SST [*Lough*, 2004].

5.2. Interannual Variability

[28] The MTM power spectrum shows significant interannual variability with periodicities of 3–4 and 6–7 years (Figure 7a). The wavelet spectrum suggests that interannual variability was strongest prior to 1920, around 1941 and again in the most recent part of the coral record (Figure 7b). Monte Carlo-SSA indicates that the 6–7 year signal is the most robust signal in the coral record (Figure 7c).

[29] The cross spectrum of coral $\delta^{18}O$ and regional SST is shown in Figure 8a. On interannual timescales, there are many narrow peaks in the coherency spectrum, but these have low confidence levels. It is unlikely that this poor relationship between annual mean coral $\delta^{18}O$ and SST is due to local windward/leeward effects (see previous section). More likely, the coral shows interannual variations in $\delta^{18}O_{sw}$ and SSS, which are not related to local temperature changes.

[30] *Rao and Sivakumar* [2003] have analyzed historical SSS data along the ship track from La Réunion to the Gulf

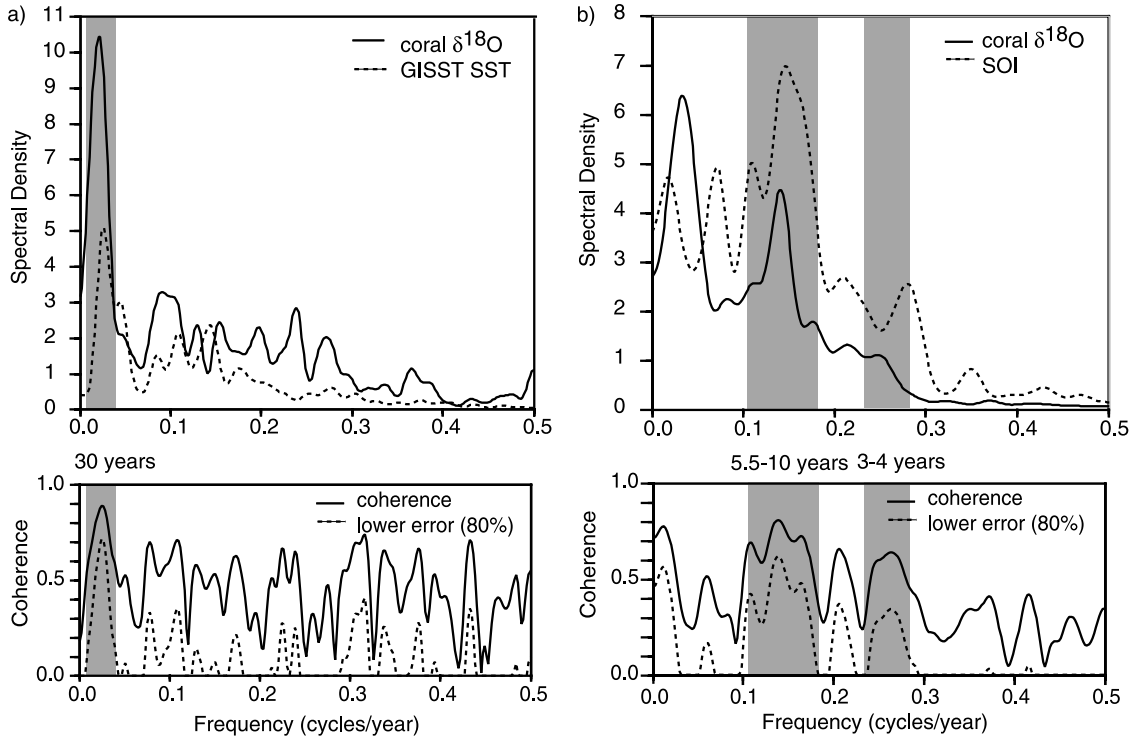

Figure 8. Blackman-Tukey cross-spectral analysis between (a) annual mean coral $\delta^{18}O$ and SST from the GISST 2.3 data set [*Parker et al.*, 1995]; time period: 1871–1995, number of lags = 62, bandwidth = 0.02. (b) Mean November–February coral $\delta^{18}O$ and mean November–February Southern Oscillation Index (SOI) [*Allan et al.*, 1991]; time period: 1866–1995, number of lags = 35, bandwidth = 0.04. All series were detrended and normalized prior to analysis.

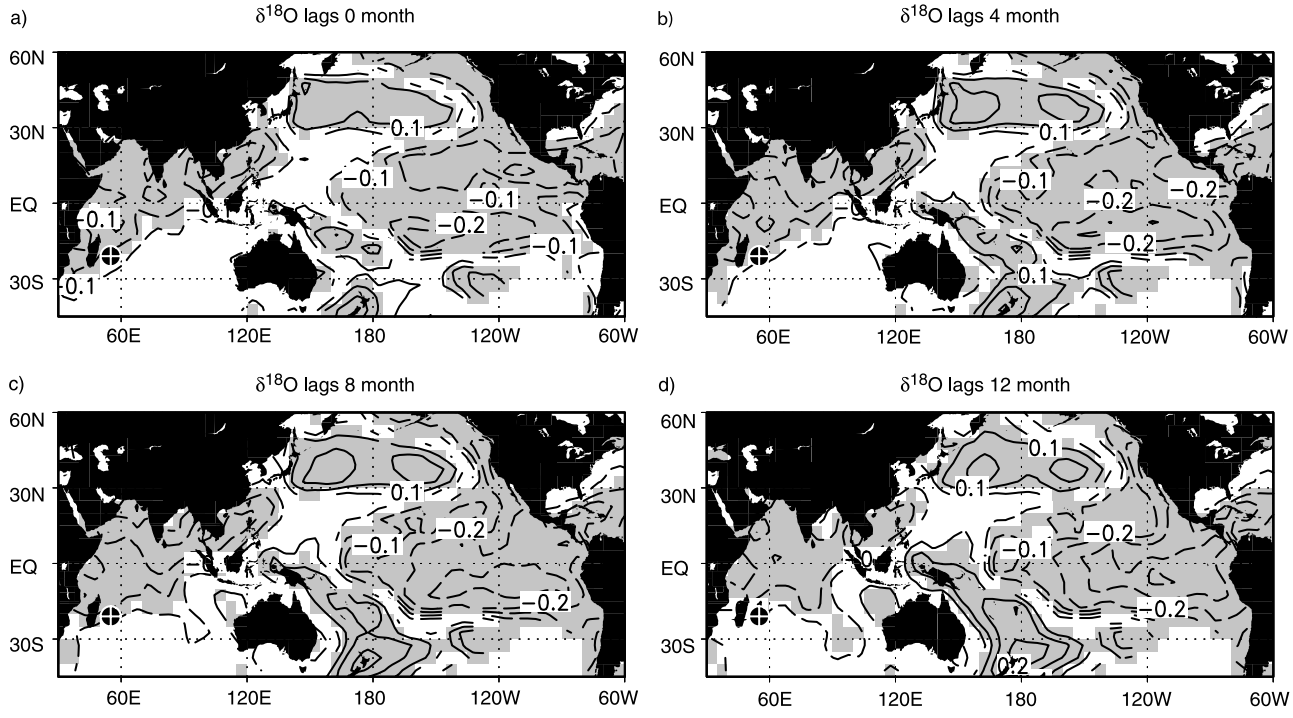

Figure 9. Correlation of the filtered 4–10 year coral $\delta^{18}O$ series with the global SST field (unfiltered) of *Kaplan et al.* [1998]. Shaded area: correlations are significant at the 5% confidence level (two sided test). Solid line: positive correlations; dashed line: negative correlations. (a) $\delta^{18}O$ lags 0 month. (b) $\delta^{18}O$ lags 4 month. (c) $\delta^{18}O$ lags 8 month. (d) $\delta^{18}O$ lags 12 month. See text for discussion.

of Aden, covering the period from 1982–1995. They reported significant interannual salinity variations, which appear to be related to ENSO. As $\delta^{18}O_{sw}$ covaries with salinity, we would also expect ENSO-related variations in $\delta^{18}O_{sw}$ in the southwestern Indian Ocean. We therefore performed a cross-spectral analysis between the November to February coral time series and the November to February Southern Oscillation Index (SOI) (taken from *Allan et al.* [1991]). Figure 8b shows that the two series are coherent at periods of 3–4 and 6–10 years.

[31] ENSO-related changes in $\delta^{18}O_{sw}$ and salinity in the vicinity of Réunion could result from: (1) variations in the P-E balance, and (2) oceanic advection. Both SSS and $\delta^{18}O_{sw}$ are a function of the local P-E balance. However, interannual variations in P-E are an order of magnitude smaller than seasonal variations (data from *Kalnay et al.* [1996]). Yet, even seasonal variations in the P-E balance only induce small variations in SSS and are not detectable in the monthly coral $\delta^{18}O$ series. Moreover, interannual variations in P-E are strongest in austral summer and mainly result from rainfall variations. However, La Réunion is situated near a zero line in the ENSO-induced rainfall anomaly pattern in the Indian Ocean sector [*Dai and Wigley*, 2000]. Noted El Niño or La Niña events are barely noticeable in the rainfall record of Réunion (Figure 3).

[32] Therefore we believe it is more likely that the interannual variations in coral $\delta^{18}O$ result from oceanic advection. In the southern Indian Ocean, the SEC carries fresher water from the eastern and central Indian Ocean toward the western margin of the basin [*Han and McCreary*, 2001]. The SEC can be seen as a westward stretching, low-salinity tongue in a region where evaporation exceeds precipitation. The Indonesian throughflow adds freshwater to the SEC, as it spreads westward by advection and diffusion [*Gordon et al.*, 1997]. Modeling of the salinity distributions in the Indian Ocean indicates that the Indonesian throughflow reduces surface salinity by 0.2 to 2 psu in a broad region of the southern hemisphere, especially from 10°S to 25°S across the Indian Ocean and near the southwestern boundary of the basin [*Han and McCreary*, 2001]. Recent observations of the Indonesian throughflow show substantial modulation of transports during ENSO, with reduced transports during El Niño, and significantly increased transports during La Niña years [*Godfrey*, 1996; *Meyers*, 1996]. The magnitude of the throughflow varies between about 2 and 15 Sv on ENSO timescales [*Meyers*, 1996]. This should also lead to ENSO-related changes in the strength of the SEC, with reduced transports in El Niño, and increased transports in La Niña years. A stronger SEC would push low salinity waters from the eastern and central Indian Ocean further toward the western margin of the basin. The zonal gradients in mean surface salinity along the path of the SEC are large. Mean SSS decreases by 0.3 to 0.4 psu from 75°E to 55°E [*Conkright et al.*, 2002]. Historical salinity data for the period from 1982 to 1995 also shows that the core of the low salinity water of the SEC expands south to Réunion during La Niña years [see *Rao and Sivakumar*, 2003, Figure 6].

[33] Figure 9 shows the correlation of the filtered 4–10 year coral time series with the (unfiltered) global SST

anomaly field from *Kaplan et al.* [1998]. The correlation was computed for successive time lags. The typical ENSO pattern emerges when coral $\delta^{18}O$ lags the global SST field by 12 month (Figure 9d). The correlations obtained are low. However, because only the coral time series was filtered, the squared correlation coefficients give the fraction of the total SST variance (all periods) captured by the 4–10 year variability of the coral. Figure 9 shows a negative correlation between the Réunion coral record and SST in the eastern equatorial Pacific when the coral lags the SST field by 12 month. We therefore propose the following mechanism: During La Niña years, the Indonesian throughflow and the southeasterly trade winds are stronger than normal, and lead to a strengthening of the SEC, which pushes low salinity water toward the western margin of the Indian Ocean basin. Although La Niña events are not as frequent as El Niño, they tend to occur approximately 12 month after an El Niño event. According to this scenario, La Niña has a strong impact on salinity in the western Indian Ocean.

[34] We are aware that there are still uncertainties associated with the proposed mechanism. For example, our interpretation requires that the age model of our coral record is absolutely correct. Furthermore, we note that the strong El Niño of 1940/41 coincides with a large negative $\delta^{18}O$ anomaly (Figure 6). However, according to *Quinn and Neal* [1992] the evolution of the 1940/41 El Niño was highly unusual. To address these problems, continuous, multiyear measurements of local SST, $\delta^{18}O_{sw}$ and SSS directly at the coral site are currently under way. Moreover, our interpretation may be confirmed with coral records from multiple sites along the path of the SEC. Several of the already published coral records from the eastern Indian Ocean should be influenced by the Indonesian throughflow to some extend, e.g., the Bali record from Indonesia [*Charles et al.*, 2003], and the Houtmann Abrolhos and Ningaloo records from western Australia [*Kuhnert et al.*, 1999, 2000]. However, all these corals are from sites with strong local ocean-atmosphere interactions (e.g., the Bali coral appears to provide an excellent record of the Indian Ocean dipole), which are also influenced by ENSO. To test our hypothesis, new corals should be collected from small islands situated directly in the low-salinity tongue of the SEC, where the westward advection of low salinity water dominates over local ocean-atmosphere interactions (e.g., Cocos Keeling, Mauritius and Tromelin). If verified, the corals may be used to monitor the freshwater flux from the Western Pacific warm pool to the Indian Ocean and into the Agulhas current system on ENSO timescales.

5.3. Multidecadal Variability

[35] There is evidence for significant (95% confidence interval) multidecadal variability with a period of 30–35 years in both the MTM and wavelet power spectrum, although Monte Carlo-SSA indicates that this peak should be viewed with some caution (Figure 7). The period of the multidecadal signal is long relative to the total length of the coral time series, with only 4.5 cycles included in the complete record, and 3 cycles in the interval from 1871 to 1995, which is covered by the GISST 2.3 SST reconstruction. However, based on a basin-wide analysis of COADS and GISST data, *Allan et al.* [1995] have shown that the Indian Ocean exhibits significant multidecadal variability in SST, mean sea level pressure, surface wind stresses, vertical motion and cloudiness, lending confidence to the reality of the multidecadal signal indicated by the coral record.

[36] Cross spectral analysis of the annual mean coral $\delta^{18}O$ and SST records indicates that the two records are coherent at multidecadal frequencies with a period of approximately 30 years (Figure 8). Within this frequency band, 72–89% of the variance is linearly correlated between the two time series. Figure 10 compares annual mean coral $\delta^{18}O$, SST and mean summer (December–April) rainfall. We smoothed the three time series with an 11-point running mean to highlight the decadal and multidecadal variability of the records. There is no obvious relationship between coral $\delta^{18}O$ and rainfall on multidecadal timescales (Figure 10). In addition, although coral $\delta^{18}O$ and SST are coherent at multidecadal timescales, the sense of the relationship is of opposite sign as expected from the coral $\delta^{18}O$/temperature relationship. The magnitude of the multidecadal variations in coral $\delta^{18}O$ is with approximately 0.1‰ well above the mean analytical uncertainty for 11-year $\delta^{18}O$ estimates (see Material and Methods). Lighter mean isotopic values, which would be indicative of higher temperatures, correspond to periods of cooler SSTs, and vice versa. This requires multidecadal variations in $\delta^{18}O_{sw}$, whereby warmer SSTs are associated with more positive, and cooler SSTs with more negative $\delta^{18}O_{sw}$, that are large enough to overprint the SST signal. The shifts in SST are on the order of 0.5°C. This requires changes in $\delta^{18}O_{sw}$ of about 0.2‰, and, converted to salinity assuming a linear relationship of 0.4–0.5‰ $\delta^{18}O$ per 1 psu, which was estimated by *Delaygue et al.* [2000], changes in salinity of 0.4–0.5 psu. Assessing the reliability of these estimates would require continuous time series of $\delta^{18}O_{sw}$ and salinity measurements from the southwestern Indian Ocean sector, as well as from our coral site. These data are currently not available, but spot measurements of $\delta^{18}O_{sw}$ and salinity from the southwestern Indian Ocean show a maximum range of 0.21‰ $\delta^{18}O$ and 0.44 psu salinity (available at http://www.giss.nasa.gov/data/o18data). *Craig and Gordon* [1965], report lower values of $\delta^{18}O_{sw}$, whereas more recent measurements generally indicate higher values [*Frew et al.*, 1995], consistent with our coral data. However, the data stems from various sites and variations in latitude and longitude may also be important.

[37] We therefore looked at historical salinity data from World Ocean Database 2001 (WOD01) [*Conkright et al.*, 2002]. Figure 11 shows salinity and temperature profiles along a section across the Mascarene Plateau (2.5°S–23°S, 54°E–64°E). We averaged the data over 1955–1975 (Figure 11a) and 1975–1995 (Figure 11b). The two time intervals correspond to one low-salinity (1955–1975) and one high-salinity (1975–1995) interval inferred from the coral record (Figure 10), and both have similar spatial and temporal data coverage. In the 1955–1975 interval, observed salinities in the center of the SEC (12°–15°S) are lower than in 1975–1995, and the 35 psu contour lies south of 20°S. In the 1975–1995 interval, the 35 psu contour shifts to the north of 20°S. Surface water temperatures are slightly higher in 1975–1995, but this may also reflect the

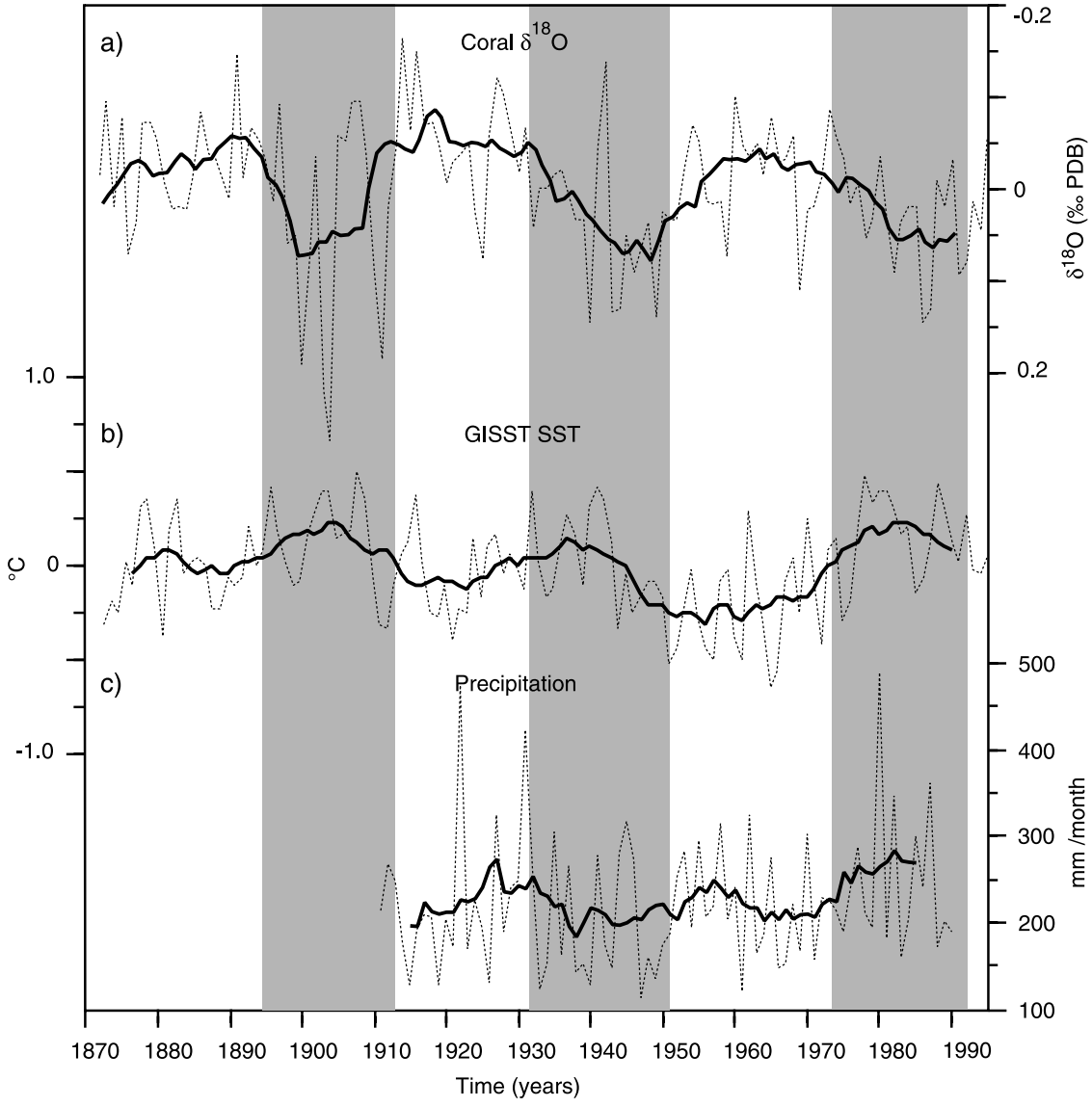

Figure 10. (a) Annual mean coral $\delta^{18}O$ (dashed line) and 11 point moving average (solid line). (b) Annual mean SST from the GISST 2.3 data set (dashed line) [*Parker et al.*, 1995] and 11 point moving average (solid line). (c) Mean summer (December–April) precipitation (dashed line) [*Hulme*, 1992] and 11 point moving average (solid line). Coral $\delta^{18}O$ and SST are shown as anomalies relative to the mean for the period 1871–1995. The long-term trend has been removed.

recent warming trend of the Indian Ocean (the linear trend has not been removed from the data).

[38] Although the magnitudes of the salinity variations indicated by the data from WOD01 are lower than those inferred from our coral record, the signs are consistent (note that the SSS changes inferred from coral $\delta^{18}O$ are peak-to-peak variations, whereas the WOD01 data has been averaged over two 20 year intervals). Thus we attribute the multidecadal salinity changes inferred from coral $\delta^{18}O$ to variations in the strength of the SEC. However, unlike interannual variations, multidecadal changes in salinity and $\delta^{18}O_{sw}$ inferred from coral $\delta^{18}O$ are associated with regional SST variations. Warmer surface temperatures always coincide with higher surface salinities and vice versa (Figure 10).

[39] What links multidecadal salinity variations of the SEC to SST changes? The southern Indian Ocean gyre is wind-driven [e.g., *Allan et al.*, 1995; *Reason et al.*, 1996]. *Allan et al.* [1995] have found significant multidecadal variations in the surface wind field of the Indian Ocean. The southern Indian Ocean gyre and the Indonesian throughflow respond to the surface wind forcing, leading to enhanced or decreased poleward transport of tropical waters via the SEC and Agulhas currents [*Reason et al.*, 1996]. Stronger surface winds spin up the subtropical gyre, and lead to a strengthening of the SEC. Stronger surface

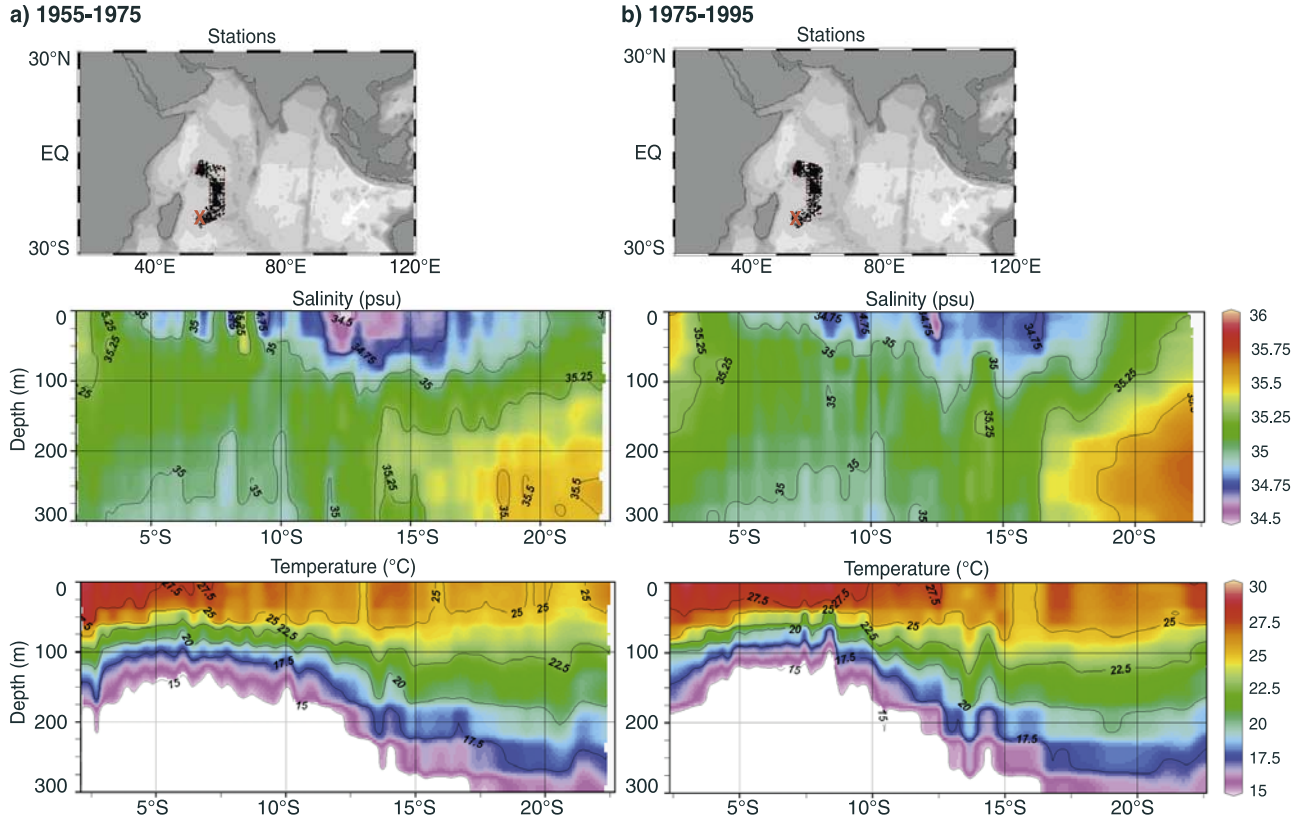

Figure 11. Historical salinity and temperature profiles across the Mascarene plateau (2.5°S–23°S, 54°E–64°E): (a) 1955–1975 and (b) 1975–1995. (top) Map showing location of stations (black dots). (middle) Salinity (psu) versus depth, bottom: temperature (°C) versus depth. Data from WOD01 [*Conkright et al.*, 2002]. Figures created with Ocean Data View (see http://www.awi-bremerhaven.de).

winds should also lead to stronger evaporation in the subtropical Indian Ocean, and colder SSTs. Hence multidecadal variations in the surface wind forcing may account for colder (warmer) SSTs together with lower (higher) surface salinities along the path of the SEC.

[40] We conclude that the coral shows multidecadal salinity variations that result from changes in the transport of the SEC and the Indonesian throughflow, which varies in response to the surface wind field over the Indian Ocean. The coral isotopic record shows that the subtropical Indian Ocean gyre and the Indonesian throughflow are important components of climate variability on multidecadal timescales.

5.4. Long-Term Trend

[41] The Réunion coral $\delta^{18}O$ record shows a long-term, uniform trend of isotopic depletion toward the present (Figure 6). The magnitude of this trend is approximately 0.7‰ since 1832, and 0.3‰ since 1870. Interpreted strictly as temperature, the trend would represent a warming of 2.2 to 2.8°C since 1871, and 3 to 3.9°C since 1832, assuming $\delta^{18}O$/temperature relationships of 0.18–0.22‰ per 1°C, which capture the wide range of published $\delta^{18}O$/temperature relationships for *Porites* corals [*Gagan et al.*, 1994; *Wellington et al.*, 1996; *Juillet-Leclerc and Schmidt*, 2001]. Interpreted strictly as salinity, the full trend in $\delta^{18}O$ would represent a freshening of 1.4 to 1.75 psu, based on a $\delta^{18}O$ versus SSS relationship of 0.4–0.5‰ $\delta^{18}O$ per 1 psu salinity [*Delaygue et al.*, 2000].

[42] However, complicating the interpretation of coral $\delta^{18}O$ in terms of external environmental forcing, changes in the rate of skeletal extension/calcification of the corals may affect the incorporation of stable oxygen isotopes [*McConnaughey*, 1989]. Lower skeletal extension rates may lead toward heavier $\delta^{18}O$ values. We note that the long-term decrease in coral $\delta^{18}O$ is indeed accompanied by an increase in skeletal extension rates from 5–8 mm/year to 10–11 mm/year. Therefore the long-term trend needs to be replicated by other corals from the same region having different growth patterns to confirm its climatic significance.

6. Summary and Conclusions

[43] On timescales longer than the seasonal cycle, the Réunion coral records variations in $\delta^{18}O_{sw}$ and salinity that are related to the transport of the SEC. Interannual variations in $\delta^{18}O_{sw}$ appear to be associated with the phase of the SOI. However, the poor coherency between coral $\delta^{18}O$ and regional SST on interannual scales suggests that these variations do not result from SST. We therefore propose that interannual variations in $\delta^{18}O_{sw}$ are due to oceanic advection.

The SEC transports fresher waters from the central and eastern Indian Ocean and the Indonesian throughflow toward the western margin of the Indian Ocean basin. Transports are larger during La Niña years, and may lower $\delta^{18}O_{sw}$ and salinity in the western portion of the basin. Our results suggest that corals from sites influenced by the SEC may be used to monitor the freshwater flux from the western Pacific toward the Indian Ocean on ENSO timescales.

[44] On multidecadal timescales, the coral record is coherent with regional SST, but the sense of this relationship is of opposite sign as expected from the coral $\delta^{18}O$/temperature relationship. Estimated multidecadal changes in $\delta^{18}O_{sw}$ are on the order of 0.2‰ and, converted to SSS, of 0.4–0.5 psu. However, unlike interannual variations, multidecadal variations in $\delta^{18}O_{sw}$ and salinity inferred from coral $\delta^{18}O$ are associated with SST variations. We suggest that multidecadal changes in both salinity and SST result from changes in the surface wind field, which modulates the transport of the south Indian Ocean gyre. Stronger surface winds will lead to enhanced evaporative cooling of SSTs, but increased westward transport low salinity waters from the eastern and central Indian Ocean toward the western margin of the basin via the SEC. Our coral record confirms modeling studies suggesting that multidecadal climate variability in the Indian Ocean may lead to modulations of the southern subtropical gyre, and increased or reduced poleward transport of low-salinity tropical waters.

[45] We conclude that coral $\delta^{18}O$ may be used to monitor variations in the freshwater balance in the Indian Ocean sector on interannual to centennial timescales. Variations in salinity and $\delta^{18}O_{sw}$ are not necessarily covariant with regional SST, and the physical processes associated with changes in $\delta^{18}O_{sw}$ on interannual and multidecadal timescales may be different. Our present data set will be improved through continuous, multiyear measurements of local SST, $\delta^{18}O_{sw}$, SSS, and additional geochemical parameters (e.g., Sr/Ca ratios), to reliably estimate the magnitude of variations in $\delta^{18}O_{sw}$ and SSS.

[46] **Acknowledgments.** We gratefully acknowledge Michael Joachimski and the University of Erlangen Stable Isotope Laboratory for performing the analysis. The members of the TESTREEF group are thanked for their help during field campaigns. Henning Kuhnert (Bremen) provided the GISST 2.3 data. We thank Jens Zinke for numerous discussions and suggestions. Chris Charles and two anonymous reviewers provided very helpful comments that greatly improved the clarity of the manuscript. This work was funded by the DFG through grant Du 129, 13-2 and Du 129, 13-3.

References

Allan, M. R., and L. A. Smith (1996), Monte Carlo SSA: Detecting oscillations in the presence of colored noise, *J. Clim.*, *9*, 33–73.

Allan, R. J., and M. R. Haylock (1993), Circulation features associated with the winter rainfall decrease in southwestern Australia, *J. Clim.*, *6*, 1356–1367.

Allan, R. J., N. Nicholls, P. D. Jones, and I. J. Butterworth (1991), A further extension of the Tahiti-Darwin SOI, early SOI results and Darwin pressure, *J. Clim.*, *4*, 743–749.

Allan, R. J., J. A. Lindesay, and C. J. C. Reason (1995), Multidecadal variability in the climate system over the Indian Ocean region during austral summer, *J. Clim.*, *8*, 1853–1873.

Charles, C. D., D. E. Hunter, and R. G. Fairbanks (1997), Interaction between the ENSO and the Asian monsoon in a coral record of tropical climate, *Science*, *277*, 925–928.

Charles, C. D., K. Cobb, M. D. Moore, and R. G. Fairbanks (2003), Monsoon-tropical ocean interaction in a network of coral records spanning the 20th century, *Mar. Geol.*, *201*, 207–222.

Cole, J. E., R. G. Fairbanks, and G. T. Shen (1993), Recent variability in the Southern Oscillation: Isotopic results from a Tarawa Atoll coral, *Science*, *260*, 1790–1793.

Conkright, M. E., et al. (2002), *World Ocean Database 2001*, vol. 1, *Introduction*, *NOAA Atlas, NESDIS 42*, edited by S. Levitus, 167 pp., U.S. Govt. Print. Off., Washington, D. C.

Craig, H., and L. I. Gordon (1965), Deuterium and oxygen 18 variations in the ocean and the marine atmosphere, in *Stable Isotopes in Oceanographic Studies and Paleotemperatures*, edited by E. Tongiorgi, pp. 9–130, Cons. Naz. di Rech., Spoleto, Italy.

Dai, A., and T. M. L. Wigley (2000), Global patterns of ENSO-induced precipitation, *Geophys. Res. Lett.*, *27*(9), 1283–1286.

Delaygue, G., J. Jouzel, and J. C. Dutay (2000), Oxygen 18-salinity relationship simulated by an oceanic general circulation model, *Earth Planet. Sci. Lett.*, *178*, 113–123.

Dettinger, M. D., M. Ghil, C. M. Strong, W. Weibel, and P. Yiou (1995), Software expedites singular-spectrum analysis of noisy time series, *Eos, Trans. AGU*, *76*(2), 12, 14, 21.

DiMarco, S. F., P. Chapman, W. D. Nowlin, P. Hacker, K. Donohue, M. Luther, G. C. Johnson, and J. Toole (2002), Volume transport and property distributions of the Mozambique channel, *Deep Sea Res. Part II*, *49*, 1481–1511.

Evans, M. N., A. Kaplan, and M. A. Cane (2000), Intercomparison of coral oxygen isotope data and historical sea surface temperature (SST): Potential for coral-based SST field reconstructions, *Paleoceanography*, *15*(5), 551–563.

Evans, M. N., A. Kaplan, and M. A. Cane (2002), Pacific sea surface temperature field reconstruction from coral $\delta^{18}O$ data using reduced space objective analysis, *Paleoceanography*, *17*(1), 1007, doi:10.1029/2000PA000590.

Frew, R. D., K. J. Heywood, and P. F. Dennis (1995), Oxygen isotope study of water masses in the Princess Elizabeth Trough, Antarctica, *Mar. Chem.*, *49*, 141–153.

Gagan, M. K., A. R. Chivas, and P.-J. Isdale (1994), High-resolution isotopic records from corals using ocean temperature and mass-spawning chronometers, *Earth Planet. Sci. Lett.*, *121*, 549–558.

Gamberoni, L., J. Geronimi, and J. F. Murail (1984), Structure hydrologique aux abords immédiats de l'île de La Réunion en période hivernale (août.–sept. 1982), *Comm. Natl. Fr. Rech. Antarct.*, *55*, 41–47.

Godfrey, J. S. (1996), The effect of the Indonesian throughflow on ocean circulation and heat exchange with the atmosphere: A review, *J. Geophys. Res.*, *101*(C5), 12,217–12,237.

Gordon, A., and J. McClean (1999), Thermohaline stratification of the Indonesian Seas—Model and observations, *J. Phys. Oceanogr.*, *29*, 198–216.

Gordon, A., S. Ma, D. Olson, P. Hacker, A. Ffield, L. Talley, D. Wilson, and M. Baringer (1997), Advection and diffusion of Indonesian throughflow water within the Indian Ocean South Equatorial Current, *Geophys. Res. Lett.*, *24*(21), 2573–2576.

Han, W., and J. P. McCreary (2001), Modeling salinity distributions in the Indian Ocean, *J. Geophys. Res.*, *106*(C1), 859–877.

Hastenrath, S., and L. Greishar (1993), The monsoonal heat budget of the hydrosphere-atmosphere system in the Indian Ocean sector, *J. Geophys. Res.*, *98*(C4), 6869–6881.

Hulme, M. (1992), A 1951–80 global land precipitation climatology for the evaluation of general circulation models, *Clim. Dyn.*, *7*, 57–72.

Juillet-Leclerc, A., and G. Schmidt (2001), A calibration of the oxygen isotope paleothermometer of coral aragonite from *Porites*, *Geophys. Res. Lett.*, *28*(21), 4135–4138.

Kalnay, E., et al. (1996), The NMC/NCAR 40-year reanalysis project, *Bull. Am. Meteorol. Soc.*, *77*, 437–471.

Kaplan, A., M. A. Cane, Y. Kushnir, A. Clement, M. Blumenthal, and B. Rajagopalan (1998), Analysis of global sea surface temperature 1856–1992, *J. Geophys. Res.*, *103*, 18,567–18,589.

Kuhnert, H., J. Pätzold, B. Hatcher, K.-H. Wyrwoll, A. Eisenhauer, L. B. Collins, and G. Wefer (1999), A 200 year coral stable oxygen isotope record from a high-latitude reef off Western Australia, *Coral Reefs*, *18*, 1–12.

Kuhnert, H., J. Pätzold, K.-H. Wyrwoll, and G. Wefer (2000), Monitoring climate variability over the past 116 years in coral oxygen isotopes from Ningaloo Reef, Western Australia, *Int. J. Earth Sci.*, *88*, 725–732.

LeBec, N., A. Juillet-Leclerc, T. Corrège, D. Blamart, and T. Delcroix (2000), A coral $\delta^{18}O$ record of ENSO driven sea surface salinity variability in Fiji (southwestern tropical Pacific), *Geophys. Res. Lett.*, *27*, 3897–3900.

Leroy, C., and O. Barbaroux (1980), Observations physiques et chimiques effectuées sur le millieu marin au tour de l'île de La Réunion, 62 pp., Inst. Sci. Tech. Peches Mar., Nantes, France.

Lough, J. M. (2004), A strategy to improve the contribution of coral data to high-resolution paleoclimatology, *Palaeogeogr. Palaeoclimatol. Palaeoecol.*, *204*, 115–143.

Mann, M. E., and J. M. Lees (1996), Robust estimation of background noise and signal detection in climatic time series, *Clim. Change*, *33*, 409–445.

McConnaughey, T. A. (1989), C-13 and O-18 isotopic disequilibria in biological carbonates: I. Patterns, *Geochim. Cosmochim. Acta*, *53*, 151–162.

Meyers, G. (1996), Variation of Indonesian throughflow and the El Niño–Southern Oscillation, *J. Geophys. Res.*, *101*(C5), 12,255–12,263.

Oberhuber, J. M. (1988), An atlas based on 'COADS' dataset: The budgets of heat, and turbulent kinetic energy at the surface of the global ocean, pp. 28, Max Planck Institut für Meteorol., Hamburg.

Paillard, D., L. Labeyrie, and P. Yiou (1996), Macintosh program performs time-series analysis, *Eos Trans. AGU*, *77*, 39.

Parker, D. E., C. K. Folland, and M. Jackson (1995), Marine surface temperature: Observed variations and data requirements, *Clim. Change*, *31*, 559–600.

Quinn, W. H., and V. T. Neal (1992), The historical record of El Niño events, in *Climate Since A. D. 1500*, edited by R. S. Bradley and P. D. Jones, pp. 623–648, Routledge, London.

Rao, R. R., and R. Sivakumar (2003), Seasonal variability of sea surface salinity and salt budget of the mixed layer of the north Indian Ocean, *J. Geophys. Res.*, *108*(C1), 3009, doi:10.1029/2001JC000907.

Reason, C. J. C. (2000), Multidecadal climate variability in the subtropics/mid-latitudes of the Southern Hemisphere oceans, *Tellus*, *Ser. A*, *25*, 203–223.

Reason, C. J. C., R. J. Allan, and J. A. Lindesay (1996), Evidence for the influence of remote forcing on interdecadal variability in the southern Indian Ocean, *J. Geophys. Res.*, *101*(C5), 1867–1882.

Reason, C. J. C., C. R. Godfred-Spenning, R. J. Allan, and J. A. Lindesay (1998), Air-sea interaction mechanisms and low-frequency climate variability in the south Indian Ocean region, *Int. J. Climatol.*, *18*, 391–405.

Ren, L., B. K. Linsley, G. M. Wellington, D. P. Schrag, and O. Hoegh-Guldberg (2002), Deconvolving the $\delta^{18}O$ seawater component from subseasonal coral $\delta^{18}O$ and Sr/Ca at Rarotonga in the southwestern subtropical Pacific for the Period 1726 to 1 997, *Geochim. Cosmochim. Acta*, *67*(9), 1609–1621.

Reynolds, R. W., and T. M. Smith (1994), Improved global sea surface temperature analysis, *J. Clim.*, *7*, 929–948.

Ropelewski, C. F., and M. S. Halpert (1987), Global and regional scale precipitation patterns associated with the El Nino/Southern Oscillation, *Mon. Weather Rev.*, *114*, 2352–2362.

Soler, O. (1997), *Atlas Climatique de la Réunion*, 80 pp., Météo-France, La Réunion, France.

Stoddart, D. R. (1971), Rainfall on Indian Ocean coral islands, *Atoll Res. Bull.*, *147*, 1–21.

Thomson, D. J. (1982), Spectrum estimation and harmonic analysis, *Proc. IEEE*, *70*, 1055–1096.

Torrence, C., and G. P. Compo (1998), A practical guide to wavelet analysis, *Bull. Am. Meteorol. Society*, *79*(1), 61–78.

Vautard, R., and M. Ghil (1989), Singular spectrum analysis in nonlinear dynamics, with applications to paleoclimatic time series, *Phys. D*, *35*, 395–424.

Wajsowicz, R. C. (2002), Air-sea interaction over the Indian Ocean due to variations in the Indonesian throughflow, *Clim. Dyn.*, *18*, 437–453.

Wajsowicz, R. C., and P. S. Schopf (2001), Oceanic influences on the seasonal cycle in evaporation rate over the Indian Ocean, *J. Clim.*, *14*, 1199–1226.

Wellington, G. M., R. B. Dunbar, and G. Merlen (1996), Calibration of stable oxygen isotope signatures in Galápagos corals, *Paleoceanography*, *11*(4), 467–480.

Woodruff, S. D., R. J. Slutz, R. L. Jenne, and P. M. Steurer (1987), A comprehensive ocean-atmosphere data set, *Bull. Am. Meteorol. Soc.*, *68*, 1239–1250.

W.-C. Dullo, M. Pfeiffer, and O. Timm, Leibniz Institut für Meereswissenschaften, IFM-GEOMAR, D-24148 Kiel, Germany. (mpfeiffer@geomar.de)

S. Podlech, Geological Survey of Denmark and Greenland, DK-1350 Copenhagen, Denmark.